The Journal of Chemical Physics

RESEARCH ARTICLE | JULY 10 2023

Equilibrium structures of selenium compounds: The torsionally flexible molecule of selenophenol

Wenqin Li ; Rizalina Tama Saragi ; Marcos Juanes ; Jean Demaison ; Natalja Vogt ; Antonio Fernández-Ramos ; Alberto Lesarri

J. Chem. Phys. 159, 024303 (2023)
https://doi.org/10.1063/5.0156413

The Journal of Chemical Physics ARTICLE pubs.aip.org/aip/jcp

Equilibrium structures of selenium compounds: The torsionally flexible molecule of selenophenol

Cite as: J. Chem. Phys. 159, 024303 (2023); doi: 10.1063/5.0156413
Submitted: 29 April 2023 • Accepted: 15 June 2023 •
Published Online: 10 July 2023

Wenqin Li,[1] Rizalina Tama Saragi,[1,a)] Marcos Juanes,[1,a)] Jean Demaison,[2,b)] Natalja Vogt,[2] Antonio Fernández-Ramos,[3,4] and Alberto Lesarri[1,b)]

AFFILIATIONS

[1] Departamento de Química Física y Química Inorgánica, Facultad de Ciencias—I.U. CINQUIMA, Universidad de Valladolid, Paseo de Belén, 7, 47011 Valladolid, Spain
[2] Faculty of Sciences, University of Ulm, 89069 Ulm, Germany
[3] Centro Singular de Investigación en Química Biológica y Materiales Moleculares (CIQUS), Campus Vida, Universidade de Santiago de Compostela, C/ Jenaro de la Fuente s/n, 15782 Santiago de Compostela, Spain
[4] Departamento de Química Física, Facultade de Química, Campus Vida, Universidade de Santiago de Compostela, Avda. das Ciencias s/n, 15782 Santiago de Compostela, Spain

[a)] **Present address:** Institut für Ionenphysik und Angewandte Physik, Universität Innsbruck, Technikerstrasse 25/4. OG, 6020 Innsbruck, Austria.
[b)] **Authors to whom correspondence should be addressed:** jean.demaison@gmail.com and alberto.lesarri@uva.es

ABSTRACT

The equilibrium structure of selenophenol has been investigated using rotational spectroscopy and high-level quantum mechanical calculations, offering electronic and structural insight into the scarcely studied selenium compounds. The jet-cooled broadband microwave spectrum was measured in the 2–8 GHz cm-wave region using broadband (chirped-pulse) fast-passage techniques. Additional measurements up to 18 GHz used narrow-band impulse excitation. Spectral signatures were obtained for six isotopic species of selenium (^{80}Se, ^{78}Se, ^{76}Se, ^{82}Se, ^{77}Se, and ^{74}Se), together with different monosubstituted ^{13}C species. The (unsplit) rotational transitions associated with the non-inverting μ_a-dipole selection rules could be partially reproduced with a semirigid rotor model. However, the internal rotation barrier of the selenol group splits the vibrational ground state into two subtorsional levels, doubling the dipole-inverting μ_b transitions. The simulation of the double-minimum internal rotation gives a very low barrier height (B3PW91: 42 cm^{-1}), much smaller than for thiophenol (277 cm^{-1}). A monodimensional Hamiltonian then predicts a huge vibrational separation of 72.2 GHz, justifying the non-observation of μ_b transitions in our frequency range. The experimental rotational parameters were compared with different MP2 and density functional theory calculations. The equilibrium structure was determined using several high-level *ab initio* calculations. A final Born–Oppenheimer (r_e^{BO}) structure was obtained at the coupled-cluster CCSD(T)_ae/cc-wCVTZ level of theory, including small corrections for the wCVTZ → wCVQZ basis set enlargement calculated at the MP2 level. The mass-dependent method with predicates was used to produce an alternative $r_m^{(2)}$ structure. The comparison between the two methods confirms the high accuracy of the r_e^{BO} structure and offers information on other chalcogen-containing molecules.

I. INTRODUCTION

Spectroscopic and computational studies of selenium compounds are scarce compared to those of the lighter elements of the chalcogen family. The reasons for its lesser interest traditionally included its toxicity, offensive odor, instability of some derivatives, and the misconception that its chemistry was similar to sulfur. However, selenium compounds have lately received more attention due to their role in organic and organometallic chemistry,[1,2] materials science, and biochemistry,[3,4] particularly selenoproteins and selenoenzymes.[5] The more complex electron configuration of selenium results in different electronic and structural properties compared to sulfur and more difficult molecular orbital computations. The diatomic bond energy of the Se–Se dichalcogen[6] (332.6 kJ mol^{-1}) and C–Se carbon-chalcogen[7] (590.4 kJ mol^{-1}) bonds is ~78%–83% weaker than for sulfur,[8,9] while the

Se–H selenol bond[10] (314.5 kJ mol^{-1}) has a closer value (91.3%) to the thiol.[11] At the same time, the bond lengths of the dichalcogen Se–Se (~2.32 Å) and carbon-chalcogen C–Se (~1.96 Å) bonds are typically 9%–13% longer than in sulfur (~2.05 Å and 1.80 Å, respectively, for S–S and C–S).[12]

Among high-resolution spectroscopic studies of selenium compounds, most studies concern hydrogen[13] and dimethyl[14] selenides. Several studies have carried out synthetic and rotational investigations for alkylated selenols (methane,[15] ethane,[16] ethene,[17] 2-propene,[18] 3-butene,[19] 3-butyne,[20] cyclopropylmethyl,[21] and propargyl[22]) and selenocyanates (ethene,[23] vinyl,[24] and propargyl[25]), focusing on their structure and intramolecular hydrogen bonds. Here, we report on the electronic properties and equilibrium structure of the aromatic selenophenol (benzeneselenol, Fig. 1), combining rotational spectroscopy and molecular orbital calculations. Selenophenol is a selenation, mild reduction, and radical reagent. The molecule is structurally analogous to phenol and thiophenol, which are characterized by the internal dynamics of the large-amplitude motion of the terminal alcohol or thiol groups. In oxygen and sulfur compounds, the low-barrier double-minimum potential of the torsional inversion splits the ground vibrational state and results in large tunneling doublings (~1560 MHz in thiophenol) and large Coriolis rovibrational perturbations in the rotational spectrum.[26–29] The determination of the tunneling splittings permits the experimental determination of the inversion barrier, which in turn can be used to gauge the theoretical methods modeling inversion. However, the torsional motion is very sensitive to the barrier height, and small chemical changes can affect the torsional doubling, as observed in the *para*-halogenated aromatic rings.[30] In selenophenol, we should expect a large decrease in the torsional barrier compared to thiophenol [277.1(3) cm^{-1}][26] and phenol [1207(18) cm^{-1}].[27–29] This fact and the presence of five isotopic species with important natural abundances (0.9%–49.6%) considerably complicate the rotational spectrum. The characterization of selenophenol will permit the establishment of the trend of inversion barriers in the chalcogens and the obtaining of the experimental data necessary for the calculation of its equilibrium structure. To date, the equilibrium structures are known only for a few selenium derivatives (CSe,[31] OCSe,[32] CSe_2,[33] and CH_2Se[34]). Rotational spectra have permitted the derivability of empirical structures for several selenols (either effective, r_0, or substitution, r_s), which, therefore, are not expected to be accurate.

The present work will facilitate the observation of intermolecular clusters involving selenophenol, where the larger polarizability of selenium will probably affect its capacity to form hydrogen bonds and other non-covalent interactions. This will allow additional comparisons with the dimers of phenol[35] and thiophenol[36] and other clusters. Finally, our experiments will test the capacity of high-level quantum mechanical calculations to provide accurate reference data for the molecule, establishing an adequate calculation level in the presence of selenium atoms and large-amplitude torsional motion. The accuracy of an *ab initio* structure depends on two issues: the treatment of electron correlation and basis set convergence. For small molecules containing first-row atoms, very high accuracy can be achieved.[37] For larger molecules with heavy atoms, the situation is less favorable because extremely large basis sets are required. Furthermore, relativistic effects have to be taken into account. In such a case, the simplest solution is to use

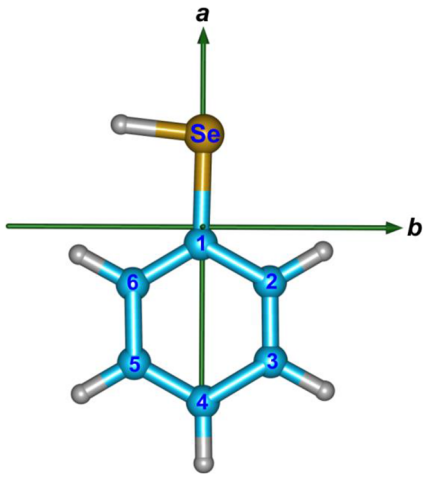

FIG. 1. Molecule of selenophenol in its principal inertial axes system.

pseudopotential basis sets[38,39] (such as cc-pwCVnZ-PP with n = T or Q), as illustrated for some mercury and zinc compounds (HgH_2[40] and ZnH_2[41]). Different calculation methods will be explored here for selenophenol.

II. COMPUTATIONAL AND EXPERIMENTAL METHODS

Selenophenol is a toxic colorless liquid (b.p. 71–72 °C) with a foul and characteristic smell, so it was manipulated with adequate precaution. The time-domain Fourier-transform microwave (FT-MW) spectroscopy experiments were conducted in jet-cooled expansions using a commercially available sample (97%). No additional purification was required. The sample is relatively volatile, so it could be vaporized at room temperature using an external reservoir inserted in the gas line. Neon at stagnation pressures of ~0.2 MPa passed through the sample, creating a pulsed supersonic jet by expansion into the evacuated (10^{-4} Pa) gas chamber. The nozzle's diameter was 0.8 mm. The FT-MW experiments used either a broadband chirped-pulse spectrometer[42] (2–8 GHz) or a Fabry–Perot resonator spectrometer[43] (8–18 GHz). The experiments differ in detection bandwidth and expansion conditions. The broadband spectrometer is based on fast-passage electric-dipole excitation using a short (4 μs) digital chirped pulse amplified up to 200 W. The transient molecular response, or free-induction decay (40 μs), is captured with a fast (25 GSamples/s) digital scope, recording the full 2–8 GHz band in every single experiment. The Fabry–Perot spectrometer uses low power (0.1 W) transform-limited pulses (1 μs) and has a resonator limited bandwidth of ~1 MHz, longer decays (400 μs), and better frequency resolution. Both spectrometers differ also in the orientation of the gas injection, which is either perpendicular (broadband) or coaxial (resonator) with the exciting radiation. The coaxial arrangement of the resonator experimental results in sub-Doppler (~10 kHz) linewidths, while the wider jet dispersion in the broadband experiment produces a linewidth of ~100 kHz. The spectrometer frequency signals are referred to as a rubidium frequency standard, and the uncertainty of the frequency

measurements is estimated to be below 5 kHz (resonator) or 20 kHz (broadband).

The computational study used different quantum mechanical methods. Most correlated-level *ab initio* electronic structure computations in the present study have been carried out at two levels: second-order Møller–Plesset perturbation theory[44] (MP2) and coupled cluster (CC) theory with single and double excitations[45] augmented by a perturbational estimate of the effects of connected triple excitations [CCSD(T)].[46] The Kohn–Sham density functional theory[47] (DFT) was also used with two hybrid Becke functionals,[48] either with Lee–Yang–Parr[49,50] (B3LYP) or Perdew–Wang[50] (B3PW91) non-local correlation. For a correct treatment of dispersion interactions, the D3 model of Grimme[51] employing the Becke–Johnson damping function (D3BJ) was used.[52] Several basis sets were used, including Pople's 6-11G and 6-311++G(d,p),[53] Ahlrich's def2-TZVP,[54] Jensen's pcs-2 and pcs-3,[55] and, for the structural optimization, the correlation-consistent polarized *n*-tuple zeta cc-pV*n*Z[56] for the hydrogen atoms, the correlation-consistent polarized weighted core-valence *n*-zeta, cc-pwCV*n*Z[57] for the carbon atoms, and the cc-pwCV*n*Z-PP[39] for the selenium atom with n = T, Q. In the following, these sets will be abbreviated as wCv*n*Z. The CCSD(T) calculations were performed with the MOLPRO[58,59] electronic structure program packages, while most other calculations utilized the GAUSSIAN programs.[60] Finally, the Atom in Molecules (AIM) theory[61,62] with its implementation in Gaussian by Cioslowski *et al.*[63–69] was used.

III. RESULTS

A. Torsional potential

As in phenol and thiophenol, the selenol group may rotate with respect to the phenyl group, and the double minimum barrier will affect the separation between the first vibrational levels and the magnitude of the torsional tunneling splitting in the spectrum. For this reason, the first task was to model the torsional potential and predict the rotational parameters. Since the experimental results are available for phenol and thiophenol, we conducted calculations on the three compounds simultaneously. The Se–H bond in the equilibrium conformation can be out-of-plane or lie in the plane of the C_6H_5-group. The latter is more plausible and consistent with a partial double bond character of the C–Se bond (see AIM results in Table I). Following initial tests with different calculation levels, we report the results using the B3PW91[48,50] density functional and the 6-311++G(d,p) basis set.[53] The torsional potentials were obtained by partial optimization of the molecular geometries at different torsions with a stepsize of 10°. Due to the symmetry of the potential for which $V\left(\frac{\pi}{2}-\phi\right)=V\left(\frac{\pi}{2}+\phi\right)$ in the interval $0\le\phi\le\frac{\pi}{2}$, and $V(\phi)=V(\phi+\pi)$ only points between 0° and 90° need to be generated. The equilibrium structures of phenol and thiophenol were found to be essentially planar, but the rotating H atom in the equilibrium structure of selenophenol deviates about 12° from planarity at this level of theory. At the saddle point (transition state), this H atom is in a perpendicular position to the ring for the three molecules. The effect of the zero-point energy (ZPE) on the torsional motion is usually neglected. However, here we have included such a contribution by transforming the force constant matrix of atomic Cartesian coordinates into a force constant matrix in non-redundant internal coordinates. To obtain the non-torsional force constant matrix,

TABLE I. Atoms-in-molecules analysis for selenophenol.

Bond	ρ (a.u.)[a]	ε[b]	Bond order
C1–C2	0.3072	0.206	1.44
C1–C6	0.3077	0.203	1.40
C2–C3	0.3094	0.209	1.40
C3–C4	0.3106	0.200	1.44
C4–C5	0.3105	0.199	1.40
C5–C6	0.3097	0.209	1.44
C2–H2	0.2831	0.023	0.99
C3–H3	0.2835	0.016	0.98
C4–H4	0.2835	0.020	1.00
C5–H5	0.2837	0.016	0.98
C–Se	0.1555	0.199	1.18
Se–H	0.1764	0.114	1.10
	Charges (a.u.)		
	C1	−0.229	
	C2	0.004	
	C3	−0.007	
	C4	−0.013	
	C5	−0.006	
	C6	0.001	
	H2	0.015	
	H3	0.020	
	H4	0.018	
	H5	0.021	
	H6	0.020	
	Se	0.284	
	H (Se)	−0.130	

[a]Electronic density in atomic units (e/Å^3).
[b]Bond ellipticity (adimensional).

we have dropped the row and column that correspond to the torsional mode and diagonalized the $(3N-7)\times(3N-7)$ matrix (N being the number of atoms). This procedure allows for obtaining the $3N-7$ non-torsional vibrational frequencies.[70] The difference in the non-torsional ZPEs, ΔE_{ZPE}, is the difference between the non-torsional ZPE at the saddle point and the equilibrium structure and is incorporated into the calculated points as a correction of the type,

$$\Delta V_{ZPE}(\phi)=\Delta e_{ZPE}[1-\cos\phi] \tag{1}$$

in the interval $0\le\phi\le\frac{\pi}{2}$. The rest of the potential is replicated by the symmetry conditions indicated above. The resulting calculated potentials were fitted to a Fourier series of the type,

$$V(\phi)=\sum_{j=0}^{N} a_{2j}\cos(2j\phi) \tag{2}$$

where a_{2j} is the fitting parameter (see Table II) and ϕ is the value of the torsional angle. The energy levels were obtained by diagonalizing the one-dimensional Schrödinger equation,

$$-\frac{\hbar^2}{2I(\phi)}\Phi(\phi)+V(\phi)\Phi(\phi)=e\Phi(\phi), \tag{3}$$

TABLE II. Predicted torsional barrier height without ($V_2^{\ddagger}$) and with non-torsional ZPE ($V_2^{\ddagger} + \Delta V_{ZPE}$), experimental values ($V_2^{exp}$), fitting parameters for Eq. (2), and reduced moments of inertia of the equilibrium (I_{eq}) and saddle-point structures ($I^{\ddagger}$) for phenol (Ph-OH), tiophenol (Ph-SH), and selenophenol (Ph-SeH).

Molecule	$V_2^{\ddagger}$ (cm^{-1})	$V_2^{\ddagger} + \Delta V_{ZPE}$ (cm^{-1})	V_2^{exp} (cm^{-1})	$V_2(\phi)$ fitting parameters (cm^{-1})	I_{eq}, $I^{\ddagger}$ (uÅ^2)
Ph-OH	1302	1276	1207(18)[a]	a_0 = 606.95 a_2 = −631.32 a_4 = 25.218	0.782 16, 0.790 97
Ph-SH	277	289	277.1(3)[b]	a_0 = 129.81 a_2 = −143.01 a_4 = 11.999	1.7179, 1.7430
Ph-SeH	42	42	N.A.[c]	a_0 = 15.166 a_2 = −19.807 a_4 = 6.184 1 a_6 = 0.518 52 a_8 = 0.763 85	2.0802, 2.0915

[a]References 27 and 28.
[b]Reference 26.
[c]Not available.

where $I(\phi)$ is the moment of inertia, $\Phi(\phi)$ is the trial wavefunction, and $V(\phi)$ is the potential given by Eq. (2). Due to the symmetry of the potential, the general trial wavefunction,

$$\Phi(\phi) = \sum_{k=-m_{max}}^{k=m_{max}} c_k e^{ik\phi}, \tag{4}$$

can be separated by symmetry into four independent wavefunctions (M_{max} is the total number of functions). Two of the wavefunctions are

$$\Phi(\phi)_\mu = \sum_{k=0}^{k=m_{max}/2} c_{2k+\mu} \cos[(2k+\mu)\phi] \tag{5}$$

and the other two are

$$\Phi'(\phi)_\mu = \sum_{k=1}^{k=\frac{m_{max}}{2}-1} c'_{2k-\mu} \sin[(2k-\mu)\phi]. \tag{6}$$

The parameter μ can take the values 0, 1, and the two wavefunctions that are symmetric with respect to the internal rotation are $\Phi(\phi)_0$ and $\Phi'(\phi)_0$, which correspond to the A_1 and A_2 symmetry species. The antisymmetric wavefunctions $\Phi(\phi)_1$ and $\Phi'(\phi)_1$ correspond to the B_2 and B_1 symmetry species, respectively, as illustrated in Fig. 2. The solution by the variational method of the Schrödinger equation employing each of four wavefunctions leads to the energy levels with the symmetry indicated (*vide supra*). A value of M_{max} = 100 is enough to obtain convergent results.

The reduced moment of inertia, $I(\phi)$, of the X–H group (X = O, S, and Se) varies along the torsional motion. We have calculated the value at the equilibrium position, I_{eq}, and at the transition state, $I^{\ddagger}$ (see Table II) by following the procedure described in Ref. 71 and implementing it as a tool in MsTor.[72] We have considered that the variation of the inverse of the moment of inertia can be described by the function

$$\frac{1}{I(\phi)} = b_0 + b_2 \cos(2\phi). \tag{7}$$

Using the above information and considering that the minima are located at $\phi = 0°, 180°$, and the saddle point at $\phi = -90°, 90°$, the coefficients of Eq. (7) are given by

$$b_0 = \frac{1}{2}\left(\frac{1}{I_{eq}} + \frac{1}{I^{\ddagger}}\right) \tag{8}$$

and

$$b_2 = \frac{1}{2}\left(\frac{1}{I_{eq}} - \frac{1}{I^{\ddagger}}\right). \tag{9}$$

The torsional barriers (V_2), vibrational energy level separation (ΔE_{01}), and the predicted rotational spectral splittings ($\Delta\nu$, ~2 × ΔE_{01}) are listed in Tables II and III. The calculated barrier height of phenol (V_2 = 1276 cm^{-1}) exceeds the experimental value [1207(18) cm^{-1}] by ~5% (or +69 cm^{-1}) within our model. As a result, the calculated splitting of phenol ($\Delta\nu$ = 62 MHz) is about half the experimental value (~112 MHz).[27,28] However, it is possible to match the experimental splitting with a small adjustment of the calculated barrier height, i.e., by lowering the predicted barrier by 127 cm^{-1} to V_2 = 1149 cm^{-1}. In that case, the barrier height is just 58 cm^{-1} below the experiment. In the case of thiophenol, the calculated barrier height (V_2 = 289 cm^{-1}) and the energy splitting (ΔE_{01} = 781 MHz) are already very close to the experimental values (V_2 = 277.1 cm^{-1}, ΔE_{01} ~ 750 MHz).[26] In this case, the ~fourfold decrease in the barrier height with respect to phenol produces large but mensurable splittings ($\Delta\nu$ ~ 1500 MHz) in the spectrum of thiophenol. In selenophenol, the estimated torsional barrier decreases abruptly to V_2 = 42 cm^{-1} and the difference between the two lowest energy levels grows to ΔE_{01} ~ 72.2 GHz (2.4 cm^{-1}),

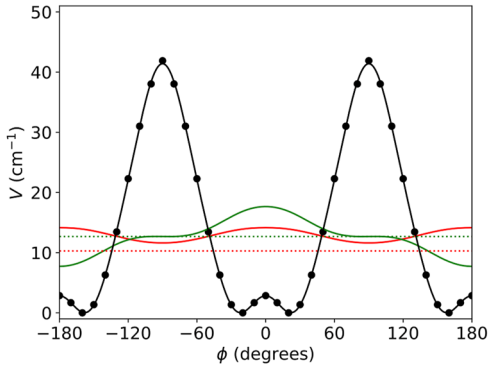

FIG. 2. Calculated potential (black points) along the torsional dihedral for selenophenol at the B3PW91/6-311++G(d,p) level. The black line represents the fitted potential to Eq. (2) (parameters of Table II), while the red and green traces represent the first torsional levels (dots) and the corresponding symmetric and antisymmetric wavefunctions (solid lines).

TABLE III. Energy of the two lowest torsional levels (cm^{-1}), the separation between these two levels (ΔE_{01}, MHz) and rotational splittings ($\Delta\nu$, MHz) according to the solutions of Eq. (3) (B3PW91/6-311++G(d,p)). The torsional splitting $\Delta\nu$ is approximately two times the energy separation ΔE_{01}. The experimental values of ΔE_{01} and $\Delta\nu$ are given in square parentheses after the calculated value.

Molecule	Level	Energy (cm^{-1})	ΔE_{01} (MHz)	$\Delta\nu$ (MHz)
Ph-OH	$v_0(A_1)$	149.037 135 6	31.4 (~56)[a]	62 (~112)[a]
	$v_1(B_2)$	149.038 183 8		
Ph-SH	$v_0(A_1)$	42.182 523 0	781 (~750)[b]	1562 [~1500][b]
	$v_1(B_2)$	42.208 560 6		
Ph-SeH	$v_0(A_1)$	10.279 724 7	72 206 (N.A.)[c]	144 412 (N.A.)
	$v_1(B_2)$	12.688 289 2		

[a]References 27 and 28.
[b]Reference 26.
[c]Not available.

much larger than the spectral bandwidth of the present experiment. Figure 2 plots the torsional potential and the splitting of the first two vibrational levels together with the representation of their wavefunctions, presenting A_1 (symmetric) and B_2 (antisymmetric) symmetries.

B. Rotational parameters

Several computational methods were employed in order to produce reliable predictions for the rotational parameters. The rotational constants and the harmonic force field were calculated at the MP2/def2-TZVP and B3LYP levels using three different basis sets: def2-TZVP, pcs-2, and pcs-3. Rather consistent results were found at the B3LYP level. At the MP2 level, the VTZ-PP, wCVTZ-PP, and wCVQZ-PP basis sets give a planar structure, whereas the cc-pVTZ-PP basis set gives an imaginary value for the lowest vibrational frequency. Furthermore, the value of the torsional frequency (ω) varies widely with the level of theory, from 34 cm^{-1} at the MP2/def2-TZVP level to 76 cm^{-1} at the B3LYP/pcs-2 level. This is probably an indication of a very anharmonic vibration, as already observed

TABLE IV. Computed spectroscopic parameters for selenophenol: rotational constants, centrifugal distortion constants, inertial defect, and lowest vibration.

Method	MP2	B3LYP		
Basis set	def2-TZVP	def2-TZVP	pcs-2	pcs-3
A (MHz)[a]	5573.62	5610.35	5611.74	5615.23
B (MHz)	960.57	962.93	962.42	963.39
C (MHz)	825.00	821.87	821.53	822.31
D_J (kHz)[b]	0.0312	0.0281	0.0269	0.0270
D_{JK} (kHz)	0.2769	0.1844	0.3095	0.3039
D_K (kHz)	0.8099	0.8971	1.1768	1.1586
d_1 (kHz)	−0.0045	−0.0048	0.0043	0.0043
d_2 (kHz)	0.0015	−0.0007	−0.0008	−0.0008
Δ (uÅ^2)[c]	−4.246	−0.363	−0.262	−0.309
ω (cm^{-1})[d]	34	64	76	69

[a]Rotational constants (A, B, *and* C).
[b]Watson's S-reduced quartic centrifugal distortion constants (D_J, D_{JK}, D_K, d_1, and d_2).
[c]Inertial defect ($\Delta = I_c - I_a - I_b = -2\sum m_i c_i^2$).
[d]Torsion frequency.

in formamide,[73] so, in this case, the MP2 method is not always reliable. The predicted rotational constants, quartic centrifugal distortion constants, inertial defects, and components of the electric dipole moment are given in Table IV. The inertial defects calculated at the B3LYP level are about −0.3 uÅ^2, a value similar to the experimental value of thiophenol,[26] −0.205 uÅ^2. The small negative value indicates the presence of a low-frequency out-of-plane vibration.[74] The anharmonic force field was calculated at the B3LYP/pcs-2 level of theory. It confirms the problems concerning the lowest torsional vibration, for which the harmonic value is 76 cm^{-1}, whereas the anharmonic value has an unphysical value of −695 cm^{-1}. This fact is mainly due to unreliable quartic force constants. On the other hand, the rovibrational corrections to the rotational constants seem to have the correct order of magnitude: ΔA = 43.0 MHz; ΔB = 5.66 MHz; and ΔC = 4.67 MHz.

C. Analysis of the rotational spectrum

The broadband spectrum of selenophenol is illustrated in Fig. 3. In the molecular jet, only the ground vibrational state is populated. As observed for phenol[28,29,75] and thiophenol,[26] the double-minimum low-barrier selenol torsion splits the ground state into two torsional sublevels ($||v = 0, \sigma\rangle$, $\sigma = 0^+, 0^-$), belonging to the totally symmetric (A_1) and permutation asymmetric (B_2) irreducible representations of the (G_4) molecular symmetry group. The torsional substates give rise to two separate stacks of rotational states, which, in a first approximation, are characterized by independent sets of rotational parameters. However, the Coriolis interaction is expected to couple the two torsional substates,[76] normally requiring a two-state torsional–rotational Hamiltonian with interaction terms. The spectrum will consist of intra-state ($0^+ \leftarrow 0^+$ and $0^- \leftarrow 0^-$) or inter-state ($0^- \leftarrow 0^+$ and $0^+ \leftarrow 0^-$) transitions, depending on the symmetry of the electric dipole moment operator. The orientation of the principal inertial axes in Fig. 1 shows that the torsional motion does not invert the μ_a component of the electric dipole moment, which belongs to A_1. As a result of the moment of transition requiring to be totally symmetric, the μ_a transitions are then

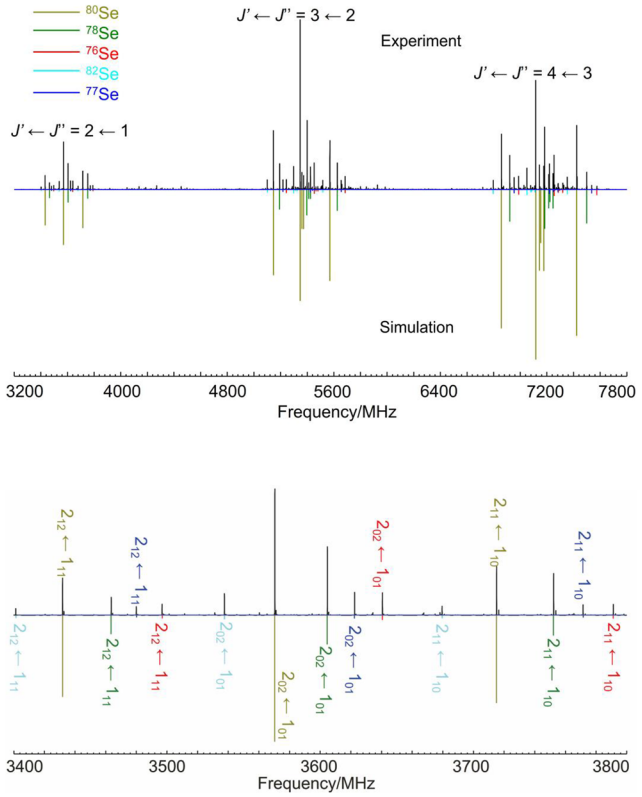

FIG. 3. Upper panel: Broadband microwave spectrum of selenophenol in the region 2–8 GHz, showing rotational transitions with $J'' = 1$–3. Lower panel: Expansion of 400 MHz illustrating isotopic satellites due to five isotopologues of the selenium atom.

intra-state. A small frequency splitting may still be expected depending on the difference between the rotational constants of the two torsional substates. Conversely, the torsional motion inverts the μ_b component, so these transitions are inter-state and are expected to show a large splitting approximately equal to twice the torsional doubling.

Three groups of transitions were first observed in the 2–8 GHz region in Fig. 3. These lines were immediately identified as R-branch ($J + 1 \leftarrow J$) μ_a transitions, with angular momentum quantum numbers $J'' = 1$–3. Later, additional transitions up to $J'' = 9$ were measured individually in the 8–18 GHz region. Depending on the line intensity, each parent (^{80}Se, 49.6%) transition is accompanied by up to five isotopic satellites in natural abundance, including ^{78}Se (23.8%), ^{76}Se (9.4%), ^{82}Se (8.7%), ^{77}Se (7.6%), and ^{74}Se (0.9%). No tunneling splittings were noticeable in the μ_a transitions. Transitions with μ_b selection rules were not assigned. The torsional splittings of these transitions were initially expected to exceed the 1.5 GHz observed in thiophenol,[26] but the results in Table IV suggest that they could reach two more orders of magnitude. Moreover, a large splitting may produce much weaker intensities for the high-energy component, making this search presently unfeasible. As a first approach, each isotopic set was fitted to a conventional semi-rigid Hamiltonian, including quartic centrifugal distortion terms.[77] Different combinations of fitting parameters were then tested. The use of five quartic distortion parameters renders a fit with a standard deviation comparable to the experiment but with a large, unrealistic D_K constant. Fixing the centrifugal distortion constants to *ab initio* values produces a bad fit, confirming the presence of coupling terms absorbed by the distortion parameters. The presence of coupling interactions is also confirmed by the fact that only transition states with pseudo-quantum numbers $K_{-1} \leq 2$ could be fitted to experimental uncertainty. Considering the small size of the present experimental dataset, only three distortion constants were fitted for the results of Table V, including the ^{80}Se, ^{78}Se, ^{76}Se, ^{82}Se, ^{77}Se, and ^{74}Se species. The experimental transition frequencies and residuals are collected in Tables S-I to S-VI (the supplementary material). In all these cases, the lack of μ_b transitions makes the largest rotational constant (A) ill-determined and the value of D_K artificially large. Additionally, the proximity of the selenium atom to the a inertial axis translates into near equal values of the A rotational constant. Monosubstituted ^{13}C isotopic satellites could be measured in natural abundance for some of the selenium species. Tables S-VII and S-VIII (the supplementary material) collect the fitted rotational parameters for the eight ^{13}C species of the ^{80}Se and ^{78}Se isotopologues. It should be noticed that substitutions in positions C(2) and C(3) break molecular symmetry, hence removing the torsional splitting. For this reason, these fittings are not directly comparable to those of ^{13}C(1) and ^{13}C(4), which corresponds to the low-frequency component of the torsional doubling. The ^{13}C transitions are collected in Tables S-IX to S-XVI (the supplementary material).

D. Equilibrium structure

1. Ab initio Born–Oppenheimer structure

The *ab initio* structure was optimized at the CCSD(T)/wCVTZ level of theory, with all electrons being correlated (ae). The small correction due to the basis set enlargement wCVTZ → wCVQZ was estimated at the MP2 level using Eq. (1),

$$r_e^{BO} = r_e[\mathrm{CCSD(T)\_ae/wCVTZ}] + r_e[\mathrm{MP2\_ae/wCVQZ}] - r_e[\mathrm{MP2\_ae/wCVTZ}]. \quad (10)$$

The accuracy of this additive method is known to be generally better than 0.001 Å.[78] The largest correction is for the C–Se bond, with a shortening of 0.003 Å. For the other bonds, the shortening is smaller than 0.002 Å. For the bond angles, the correction is almost negligible, with the largest value being for the ∠(C1SeH) angle, which is lengthened by 0.1°. This structure is given in Table VI. The equilibrium rotational constants calculated with this structure (B_e^{BO} = 970.3 MHz and C_e^{BO} = 827.0 MHz) are in good agreement with the semi-experimental rotational constants obtained by correcting the ground state rotational constants with the rovibrational corrections: B_e^{SE} = 969.9 MHz and C_e^{SE} = 827.3 MHz. However, as explained above, because of the presence of rovibrational effects that could not be accounted for with the present experimental data, the agreement is not good for the A-rotational constant (A_e^{BO} = 5601.8 MHz and A_e^{SE} = 5643.8 MHz).

TABLE V. Experimental rotational parameters for the six most abundant isotopologues of selenophenol.

	^{80}Se	^{78}Se	^{76}Se	^{82}Se	^{77}Se	^{74}Se
A (MHz)[a]	5589.1(19)[b]	5591.6(19)	5586.6(16)	5589.9(17)	5588.9(13)	5575.0(10)
B (MHz)	964.1847(38)	974.1706(35)	984.6200(24)	954.6611(28)	979.3251(22)	995.5793(40)
C (MHz)	822.6092(42)	829.8609(40)	837.4260(27)	815.6471(27)	833.5915(24)	845.3304(42)
D_J (kHz)	0.249(30)	0.347(30)	0.284(32)	0.259(27)	0.244(27)	0.48(17)
D_{JK} (kHz)	23.68(90)	21.92(75)	24.20(56)	23.28(35)	23.90(50)	23.71(86)
D_K (kHz)	−5728.(578)	−5603.(506)	−6182.(497)	−5563.(589)	−5515.(423)	−9040.(293)
d_1 (kHz)	[0.0]	[0.0]	[0.0]	[0.0]	[0.0]	[0.0]
d_2 (kHz)	[0.0]	[0.0]	[0.0]	[0.0]	[0.0]	[0.0]
σ (kHz)[c]	63.6	54.1	30.0	39.8	30.7	8.9
N[d]	40	37	30	35	33	13

[a]Rotational parameters as defined in Table IV.
[b]Standard deviation in units of the last digit. The calculated errors do not reflect the uncertainties associated with the limitations of the semirigid Hamiltonian for this molecule and the limited dataset.
[c]Standard deviation of the fit.
[d]Number of fitted transitions.

TABLE VI. Molecular structure of selenophenol (distances in Å, angles in degrees).

	r_e^{BO}[a]	$r_m^{(2)}$[b]
r(SeH)	1.4578(40)	1.4579(32)
r(CSe)	1.9067(50)	1.8943(11)
r(C3C4)	1.3933(20)	1.3942(15)
r(C4C5)	1.3913(20)	1.3941(6)
r(C5C6)	1.3910(20)	1.3945(12)
r(C6C7)	1.3913(20)	1.3934(12)
r(C7C8)	1.3905(20)	1.3928(6)
r(C4H)	1.0811(20)	1.0812(16)
r(C5H)	1.0811(20)	1.0809(16)
r(C6H)	1.0804(20)	1.0802(16)
r(C7H)	1.0810(20)	1.0810(16)
r(C8H)	1.0819(20)	1.0820(16)
∠(HSeC)	94.57(30)	94.69(24)
∠(SeC3C4)	122.50(30)	122.27(12)
∠(C3C4C5)	119.80(30)	120.85(10)
∠(C4C5C6)	120.50(30)	120.50(7)
∠(C5C6C7)	119.51(30)	119.52(3)
∠(C6C7C8)	120.37(30)	120.38(7)
∠(C3C4H)	120.32(30)	120.23(24)
∠(C4C5H)	119.37(30)	119.30(24)
∠(C5C6H)	120.24(30)	120.28(24)
∠(C6C7H)	120.16(30)	120.23(24)
∠(C7C8H)	119.88(30)	119.93(24)

[a]See Table S-XVII and Eq. (10). The uncertainties in parentheses are used for the weighting of the predicates; see the text.
[b]With C_b = 6.58(40) u$^{1/2}$Å; C_c = 7.54(82) u$^{1/2}$Å; d_b = −3.72(24) u$^{1/2}$Å^2; and d_c = −4.56(49) u$^{1/2}$Å^2.

2. Mass-dependent structure

The most interesting part of the structure is around the ipso angle. Unfortunately, the Cartesian coordinates of the C1 carbon atom are small: a = −0.282 Å and b = 0.028 Å. Furthermore, the b-coordinate of the Se atom is also quite small (−0.019 Å). For these reasons, it is not possible to determine a reliable substitution structure.[79] Moreover, the anharmonic force field is perhaps not reliable enough and, therefore, cannot be used to calculate the small variations of the rovibrational corrections upon isotopic substitution. To avoid this difficulty, the structure was calculated using the Watson's mass-dependent, or r_m method,[80] where the moments of inertia along the principal inertial axes (g = a, b, c) are approximated as

$$I_g^0 = I_g^m + c_g\sqrt{I_g^m} + d_g\left[\frac{\prod_i m_i}{m}\right]^{1/(2N-2)}, \quad (11)$$

where I_g^0 denotes the ground-state moments of inertia, I_g^m are the moments of inertia calculated from the r_m parameters, c_g and d_g are the fitting parameters (one for each axis), M is the total molecular mass, m_i is the atomic mass, and N is the number of atoms. When the last term is neglected, this equation leads to the so-called $r_m^{(1)}$ structure, and when the second correction term is retained (with the coefficient d_g), it gives the $r_m^{(2)}$ structure. This second term is important in the presence of small coordinates, which is the case here.

The mass-dependent method requires the determination of three to six additional parameters, which often significantly worsens the fit. This explains why the r_m method is rarely successful for a moderately large molecule. However, it was shown in the case of diphenyldisulfide,[81] diallydisulfide,[82] ethynylcyclohexane,[83] and other moderately large molecules such as fructose[84] that the predicate or mixed estimation method[85,86] gives a structure whose quality is comparable to that of the traditional semi-experimental method. For the predicates, the r_e^{BO} structure was used with conservative uncertainties, which are given in Table VI. As the A-rotational constants seem to be perturbed, they were not used in the fit. The final $r_m^{(2)}$-structure also is given in Table VI. The comparison with the computed r_e^{BO} parameters (in the same Table) gives a maximum absolute deviation (MAD) of 0.0006 Å for the bond lengths, the largest deviation being 0.013 Å for the C1–Se bond. The r_e^{BO} value of

TABLE VII. Molecular structure of the selenol group in some selenium derivatives.

Molecule	Type[a]	r(C–Se) (Å)	r(Se–H) (Å)	∠(CSeH) (deg)	References
Phe-SeH	r_e	1.907	1.458	94.57	This work
H_2Se	r_e		1.459	90.8	13
CH_3CH_2SeH *trans*	r_s	1.962(2)	1.440(10)	93.5(6)	16
CH_3CH_2SeH *gauche*	r_s	1.957(4)	1.467(4)	93.1(3)	16
CH_3SeH	r_s	1.959(10)	1.473	95.45	15
$(CH_3)_2Se$	r_s	1.945			14
H_2C = CHSeH *syn*	MP2	1.895	1.460	94.3	17
H_2C = $CH(CH_2)_2SeH$	MP2	1.953	1.462	94.26	19

[a]Equilibrium and substitution structures are denoted, respectively, r_e and r_s.

this bond is probably slightly too long because convergence is not yet achieved with the cc-pwCVQZ-PP basis set. However, as noted previously, the Cartesian coordinates of the atoms Se and C1 are quite small, and for this reason, it is difficult to obtain an accurate bond length. Furthermore, the comparison of the experimental C–Se bond lengths in other molecules, presented in Table VII, indicates that the BO value is likely to be more accurate. For the bond angles, the MAD is only 0.06°, the mean absolute error is 0.16°, and the largest deviation, 1.05°, is for the angle ∠(C3C4C5) opposite to Se. It may be explained by the fact that the C4 atom has a very small b coordinate: −0.003 Å. In conclusion, these results are in favor of the accuracy of the r_e^{BO} structure.

IV. CONCLUSION

The torsionally flexible molecule selenophenol was studied using computational methods and rotational spectroscopy. The rotational spectrum revealed a large number of isotopologues in natural abundance, associated with the six selenium isotopic species detectable for the parent (^{12}C) and some monosubstituted ^{13}C species. While rotational parameters were derived for all observed species, the huge tunneling splitting associated with the selenol torsion presently prevented the determination of the experimental torsional barrier and the Coriolis coupling interaction terms. The torsional barrier was estimated using DFT calculations (B3PW91/6-311++G(d,p)) including zero-point energy (ZPE) on the torsional motion, which predict a low barrier of 42 cm^{-1} and tunneling splittings of ΔE_{01} = 72 GHz.

Several molecular structures were calculated for selenophenol, including equilibrium and mass-dependent geometries. These calculations permit a comparison with other chalcogen-containing molecules. For aromatic molecules, when the substituent is a π-electron donor, it is expected that the ipso angle is less than 120° and that the C1–C2 and the C2–H bonds are larger than the values found in benzene.[87,88] We found this same tendency in selenophenol, despite the small changes: ∠(C6C1C2) = 119.89°, r(C3 = C4) = 1.394 Å, and r(C2–H) = 1.082 Å, compared to r(C1 = C2) = 1.391 Å and r(C2–H) = 1.080 Å in benzene.[89] The other bond lengths are closer to the values found for benzene. The opposite behavior is found for phenol,[90] but, contrary to the selenium atom, the oxygen atom has a negative charge. These results are confirmed by the AIM analysis of Table I, performed at the B3LYP/6-311++G(d,p) level of theory with the r_e^{BO} equilibrium structure. Indeed, the electronic density ρ is slightly smaller for the bonds C1 = C2, C1 = C6, and C2–H. Furthermore, the charge on the selenium atom at 0.285 a.u. is positive.

Another interesting result of the AIM analysis is the value of the bond ellipticity ε for the C1–Se bond. At 0.199, it is close to the values found for the C=C bonds (around 0.20), and it indicates a non-negligible π-character for the bond. This is confirmed by the bond order, which is larger than 1. Consequently, the bond length should be shorter than for a single bond. This is difficult to check with certainty because there is no known equilibrium value for the C–Se bond. However, an empirical value for the C–Se bond length was determined for several molecules (see Table VII), and it seems to confirm that the C–Se bond in selenophenol is slightly shorter than in molecules where this bond has more single bond character.

The sum of the van der Waals radii of the H atom (1.20 Å) and the aromatic carbon (1.70 Å) is 2.90 Å, whereas the distances between the H atom of the selenol group and the two closest carbon atoms (C3C4) are 2.491 and 2.790 Å (the shortest distance of the H atom to the CC bond is 2.40 Å). It confirms that the most stable form of this compound is stabilized by a weak intramolecular hydrogen bond formed between the H atom of the selenol group and the π electrons of the CC bond. A similar behavior was previously found in etheneselenol,[17] buteneselenol,[19] and several other selenols.[22]

The results of the present study will facilitate further rotational–computational studies for other compounds and molecular complexes containing selenium, enlarging the structural information on the chalcogen group.

SUPPLEMENTARY MATERIAL

Tables S-I to S-XVI contain additional computational and experimental data.

ACKNOWLEDGMENTS

This work was supported by the Dr. B. Mez-Starck Foundation (Germany). W.L., R.T.S., M.J., and A.L. acknowledge the funding from the European Regional Development Fund (ERDF) and the

Ministerio de Ciencia e Innovación (Grant No. PID2021-125015NB-I00) and *Junta de Castilla y León* (Grant Nos. INFRARED IR2020-1-UVa02 and INFRARED IR2021-UVa13). A.F.-R. thanks the *Centro de Supercomputación de Galicia* (CESGA) for the use of their computational facilities, *Consellería de Cultura, Educación e Ordenación Universitaria* (Centro singular de investigación de Galicia acreditación 2019–2022, ED431G 2019/03, and *Grupo de Referencia Competitiva* ED431C 2021/40), the European Regional Development Fund (ERDF), and the *Ministerio de Ciencia e Innovación* through Grant No. PID2019-107307RB-I00. W.L. thanks the China Scholarship Council (CSC) for a scholarship.

AUTHOR DECLARATIONS

Conflict of Interest

The authors have no conflicts to disclose.

Author Contributions

Wenqin Li: Formal analysis (equal); Investigation (equal); Software (equal); Validation (equal); Visualization (equal). **Rizalina Tama Saragi**: Formal analysis (equal); Investigation (equal); Software (equal); Validation (equal); Visualization (equal). **Marcos Juanes**: Formal analysis (equal); Investigation (equal); Software (equal); Validation (equal); Visualization (equal). **Jean Demaison**: Conceptualization (equal); Data curation (equal); Formal analysis (equal); Investigation (equal); Methodology (equal); Software (equal); Supervision (equal); Validation (equal); Visualization (equal); Writing – original draft (equal); Writing – review & editing (equal). **Natalja Vogt**: Formal analysis (equal); Investigation (equal); Methodology (equal); Software (equal); Validation (equal); Visualization (equal); Writing – original draft (equal). **Antonio Fernández-Ramos**: Formal analysis (equal); Investigation (equal); Methodology (equal); Software (equal); Validation (equal); Visualization (equal); Writing – original draft (equal); Writing – review & editing (equal). **Alberto Lesarri**: Conceptualization (equal); Data curation (equal); Formal analysis (equal); Funding acquisition (equal); Investigation (equal); Methodology (equal); Project administration (equal); Resources (equal); Software (equal); Supervision (equal); Validation (equal); Visualization (equal); Writing – original draft (equal); Writing – review & editing (equal).

DATA AVAILABILITY

The data that support the findings of this study are available within the article and its supplementary material.

REFERENCES

[1] A. J. Mukherjee, S. S. Zade, H. B. Singh, and R. B. Sunoj, Chem. Rev. **110**, 4357 (2010).
[2] V. K. Jain, in *Organoselenium Compounds in Biology and Medicine: Synthesis, Biological and Therapeutic Treatments*, edited by V. K. Jain and K. I. Priyadarsini (Royal Society of Chemistry, Cambridge, 2017), pp. 1–33.
[3] A. Böck, K. Forchhammer, J. Heider, W. Leinfelder, G. Sawers, B. Veprek, and F. Zinoni, Mol. Microbiol. **5**, 515 (1991).
[4] M. Birringer, S. Pilawa, and L. Flohé, Nat. Prod. Rep. **19**, 693 (2002).
[5] L. A. Wessjohann, A. Schneider, M. Abbas, and W. Brandt, Biol. Chem. **388**, 997 (2007).
[6] J. Drowart and S. Smoes, J. Chem. Soc., Faraday Trans. 2 **73**, 1755 (1977).
[7] S. Smoes and J. Drowart, J. Chem. Soc., Faraday Trans. 2 **73**, 1746 (1977).
[8] K. P. Huber and G. Herzberg, *Molecular Spectra and Molecular Structure* (Springer US, Boston, MA, 1979).
[9] P. Coppens, J. C. Reynaert, and J. Drowart, J. Chem. Soc., Faraday Trans. 2 **75**, 292 (1979).
[10] S. T. Gibson, J. P. Greene, and J. Berkowitz, J. Chem. Phys. **85**, 4815 (1986).
[11] J. W. Johns and D. Ramsay, Can. J. Phys. **39**, 210 (1961).
[12] N. Vogt and J. Vogt, *Structure Data of Free Polyatomic Molecules* (Springer International Publishing, Cham, 2019).
[13] O. N. Ulenikov, E. S. Bekhtereva, N. A. Sanzharov, and P. Jensen, J. Mol. Spectrosc. **227**, 1 (2004).
[14] G. K. Pandey and H. Dreizler, Z. Naturforsch., A **32**, 482 (1977).
[15] C. H. Thomas, J. Chem. Phys. **59**, 70 (1973).
[16] J. Nakagawa, H. Okutani, and M. Hayashi, J. Mol. Spectrosc. **94**, 410 (1982).
[17] D. Petitprez, J. Demaison, G. Wlodarczak, E. H. Riague, and J.-C. Guillemin, J. Phys. Chem. A **108**, 47 (2004).
[18] H. Møllendal, A. Konovalov, and J. C. Guillemin, J. Phys. Chem. A **113**, 6342 (2009).
[19] D. Petitprez, J. Demaison, G. Wlodarczak, J. C. Guillemin, and H. Møllendal, J. Phys. Chem. A **108**, 1403 (2004).
[20] H. Møllendal, R. Mokso, and J.-C. Guillemin, J. Phys. Chem. A **112**, 3053 (2008).
[21] G. C. Cole, H. Møllendal, and J.-C. Guillemin, J. Phys. Chem. A **110**, 2134 (2006).
[22] H. Møllendal, A. Konovalov, and J.-C. Guillemin, J. Phys. Chem. A **114**, 5537 (2010).
[23] H. Møllendal and J.-C. Guillemin, J. Phys. Chem. A **111**, 7073 (2007).
[24] H. Møllendal, S. Samdal, A. J. C. Bunkan, and J.-C. Guillemin, J. Phys. Chem. A **116**, 4074 (2012).
[25] H. Møllendal, R. Mokso, and J.-C. Guillemin, J. Phys. Chem. A **113**, 2821 (2009).
[26] N. W. Larsen and L. Schulz, J. Mol. Struct. **920**, 30 (2009).
[27] T. Pedersen, N. W. Larsen, and L. Nygaard, J. Mol. Struct. **4**, 59 (1969).
[28] N. W. Larsen, E. Mathier, A. Bauder, and H. H. Günthard, J. Mol. Spectrosc. **47**, 183 (1973).
[29] G. Berden, W. L. Meerts, M. Schmitt, and K. Kleinermanns, J. Chem. Phys. **104**, 972 (1996).
[30] N. W. Larsen, J. Mol. Struct. **144**, 83 (1986).
[31] F. J. Lovas and E. Tiemann, J. Phys. Chem. Ref. Data **3**, 609 (1974).
[32] M. Leguennec, G. Wlodarczak, J. Demaison, H. Bürger, M. Litz, and H. Willner, J. Mol. Spectrosc. **157**, 419 (1993).
[33] H. Bürger and H. Willner, J. Mol. Spectrosc. **128**, 221 (1988).
[34] H. Bürger, J. Demaison, P. Dréan, W. Jerzembeck, I. Merke, and W. Stahl, Ber. Bunsenges. Phys. Chem. **102**, 872 (1998).
[35] N. A. Seifert, A. L. Steber, J. L. Neill, C. Pérez, D. P. Zaleski, B. H. Pate, and A. Lesarri, Phys. Chem. Chem. Phys. **15**, 11468 (2013).
[36] R. T. Saragi, M. Juanes, C. Pérez, P. Pinacho, D. S. Tikhonov, W. Caminati, M. Schnell, and A. Lesarri, J. Phys. Chem. Lett. **12**, 1367 (2021).
[37] M. Heckert, M. Kállay, D. P. Tew, W. Klopper, and J. Gauss, J. Chem. Phys. **125**, 044108 (2006).
[38] K. A. Peterson, D. Figgen, E. Goll, H. Stoll, and M. Dolg, J. Chem. Phys. **119**, 11113 (2003).
[39] K. A. Peterson and K. E. Yousaf, J. Chem. Phys. **133**, 174116 (2010).
[40] P. Botschwina, P. Sebald, D. Figgen, and H. Stoll, Mol. Phys. **105**, 1193 (2007).
[41] P. Sebald, H. Vennekate, R. Oswald, P. Botschwina, and H. Stoll, Mol. Phys. **108**, 487 (2010).
[42] G. B. Park and R. W. Field, J. Chem. Phys. **144**, 000001 (2016).
[43] T. J. Balle and W. H. Flygare, Rev. Sci. Instrum. **52**, 33 (1981).
[44] C. Møller and M. S. Plesset, Phys. Rev. **46**, 618 (1934).
[45] G. D. Purvis and R. J. Bartlett, J. Chem. Phys. **76**, 1910 (1982).
[46] K. Raghavachari, G. W. Trucks, J. A. Pople, and M. Head-Gordon, Chem. Phys. Lett. **157**, 479 (1989).

[47]W. Kohn and L. J. Sham, Phys. Rev. **140**, A1133 (1965).
[48]A. D. Becke, Phys. Rev. A **38**, 3098 (1988).
[49]C. Lee, W. Yang, and R. G. Parr, Phys. Rev. B **37**, 785 (1988).
[50]A. D. Becke, J. Chem. Phys. **98**, 5648 (1993).
[51]S. Grimme, J. Comput. Chem. **27**, 1787 (2006).
[52]S. Grimme, S. Ehrlich, and L. Goerigk, J. Comput. Chem. **32**, 1456 (2011).
[53]R. Krishnan, J. S. Binkley, R. Seeger, and J. A. Pople, J. Chem. Phys. **72**, 650 (1980).
[54]F. Weigend and R. Ahlrichs, Phys. Chem. Chem. Phys. **7**, 3297 (2005).
[55]F. Jensen, J. Chem. Theory Comput. **11**, 132 (2015).
[56]T. H. Dunning, J. Chem. Phys. **90**, 1007 (1989).
[57]K. A. Peterson and T. H. Dunning, J. Chem. Phys. **117**, 10548 (2002).
[58]H.-J. Werner, P. J. Knowles, G. Knizia, F. R. Manby, and M. Schütz, WIREs Comput. Mol. Sci. **2**, 242 (2012).
[59]H.-J. Werner, P. J. Knowles, P. Celani, W. Györffy, A. Hesselmann, D. Kats, G. Knizia, A. Köhn, T. Korona, D. Kreplin, R. Lindh, Q. Ma, F. R. Manby, A. Mitrushenkov, G. Rauhut, M. Schütz, K. R. Shamasundar, T. B. Adler, R. D. Amos, S. J. Bennie, A. Bernhardsson, A. Berning, J. A. Black, P. J. Bygrave, R. Cimiraglia, D. L. Cooper, D. Coughtrie, M. J. O. Deegan, A. J. Dobbyn, K. Doll and M. Dornbach, F. Eckert, S. Erfort, E. Goll, C. Hampel, G. Hetzer, J. G. Hill, M. Hodges and T. Hrenar, G. Jansen, C. Köppl, C. Kollmar, S. J. R. Lee, Y. Liu, A. W. Lloyd, R. A. Mata, A. J. May, B. Mussard, S. J. McNicholas, W. Meyer, T. F. Miller III, M. E. Mura, A. Nicklass, D. P. O'Neill, P. Palmieri, D. Peng, K. A. Peterson, K. Pflüger, R. Pitzer, I. Polyak, M. Reiher, J. O. Richardson, J. B. Robinson, B. Schröder, M. Schwilk and T. Shiozaki, M. Sibaev, H. Stoll, A. J. Stone, R. Tarroni, T. Thorsteinsson, J. Toulouse, M. Wang, M. Welborn and B. Ziegler, MOLPRO, version 2019.2, a package of *ab initio* programs (2019).
[60]M. J. Frisch, G. W. Trucks, H. B. Schlegel, G. E. Scuseria, M. A. Robb, J. R. Cheeseman, G. Scalmani, V. Barone, G. A. Petersson, H. Nakatsuji, X. Li, M. Caricato, A. V. Marenich, J. Bloino, B. G. Janesko, R. Gomperts, B. Mennucci, H. P. Hratchian, J. V. Ortiz, A. F. Izmaylov, J. L. Sonnenberg, D. Williams-Young, F. Ding, F. Lipparini, F. Egidi, J. Goings, B. Peng, A. Petrone, T. Henderson, D. Ranasinghe, V. G. Zakrzewski, J. Gao, N. Rega, G. Zheng, W. Liang, M. Hada, M. Ehara, K. Toyota, R. Fukuda, J. Hasegawa, M. Ishida, T. Nakajima, Y. Honda, O. Kitao, H. Nakai, T. Vreven, K. Throssell, J. A. Montgomery, Jr., J. E. Peralta, F. Ogliaro, M. J. Bearpark, J. J. Heyd, E. N. Brothers, K. N. Kudin, V. N. Staroverov, T. A. Keith, R. Kobayashi, J. Normand, K. Raghavachari, A. P. Rendell, J. C. Burant, S. S. Iyengar, J. Tomasi, M. Cossi, J. M. Millam, M. Klene, C. Adamo, R. Cammi, J. W. Ochterski, R. L. Martin, K. Morokuma, O. Farkas, J. B. Foresman, and D. J. Fox, Gaussian 16, Revision C.01 (Gaussian, Inc., Wallingford, CT, 2016).
[61]R. F. W. Bader, *Atoms in Molecules, A Quantum Theory* (Clarendon Press, 1994).
[62]R. J. Gillespie and P. L. A. Popelier, *Chemical Bonding and Molecular Geometry* (Oxford University Press, Oxford, 2001).
[63]J. Cioslowski and S. T. Mixon, J. Am. Chem. Soc. **113**, 4142 (1991).
[64]J. Cioslowski, Chem. Phys. Lett. **194**, 73 (1992).
[65]J. Cioslowski and P. R. Surján, J. Mol. Struct. THEOCHEM **255**, 9 (1992).
[66]J. Cioslowski, A. Nanayakkara, and M. Challacombe, Chem. Phys. Lett. **203**, 137 (1993).
[67]J. Cioslowski and A. Nanayakkara, Chem. Phys. Lett. **219**, 151 (1994).
[68]J. Cioslowski and B. B. Stefanov, Mol. Phys. **84**, 707 (1995).
[69]B. B. Stefanov and J. Cioslowski, J. Comput. Chem. **16**, 1394 (1995).
[70]J. Zheng and D. G. Truhlar, J. Chem. Theory Comput. **9**, 1356 (2013).
[71]J. E. Kilpatrick and K. S. Pitzer, J. Chem. Phys. **17**, 1064 (1949).
[72]J. Zheng, R. Meana-Pañeda, and D. G. Truhlar, Comput. Phys. Commun. **184**, 2032 (2013).
[73]G. Fogarasi and P. G. Szalay, J. Phys. Chem. A **101**, 1400 (1997).
[74]T. Oka, J. Mol. Struct. **352–353**, 225 (1995).
[75]N. W. Larsen and F. M. Nicolaisen, J. Mol. Struct. **22**, 29 (1974).
[76]D. Papousek and M. R. Aliev, *Molecular Vibrational-Rotational Spectra - Studies in Physical and Theoretical Chemistry* (Elsevier, Amsterdam, 1982), Vol. 17.
[77]J. K. G. Watson, in *Vib. Spectra Struct.*, edited by J. R. Durig (Elsevier B.V., Amsterdam, 1977), Vol. 6, pp. 1–89
[78]J. Demaison and N. Vogt, *Accurate Structure Determination of Free Molecules*, *Lectures Notes in Chemistry* (Springer International Publishing, Cham, 2020), Vol. 105, Chap. 2.
[79]J. Demaison and H. D. Rudolph, J. Mol. Spectrosc. **215**, 78 (2002).
[80]J. K. G. Watson, A. Roytburg, and W. Ulrich, J. Mol. Spectrosc. **196**, 102 (1999).
[81]J. Demaison, N. Vogt, R. T. Saragi, M. Juanes, H. D. Rudolph, and A. Lesarri, ChemPhysChem **20**, 366 (2019).
[82]J. Demaison, N. Vogt, R. T. Saragi, M. Juanes, H. D. Rudolph, and A. Lesarri, Phys. Chem. Chem. Phys. **21**, 19732 (2019).
[83]N. Vogt, J. Demaison, H. D. Rudolph, M. Juanes, J. Fernández, and A. Lesarri, J. Chem. Phys. **148**, 000001 (2018).
[84]N. Vogt, J. Demaison, E. J. Cocinero, P. Écija, A. Lesarri, H. D. Rudolph, and J. Vogt, Phys. Chem. Chem. Phys. **18**, 15555 (2016).
[85]L. S. Bartell, D. J. Romenesko, and T. C. Wong, *Chem. Soc. Spec. Period. Rep. - No. 20*, edited by G. A. Sim and L. E. Sutton (The Royal Society of Chemistry, London, 1975), p. 72.
[86]J. Demaison, in *Equilibrium Molecular Structures*, edited by J. Demaison, J. E. Boggs, and A. G. Csaszar (CRC Press, Boca Raton, FL, 2011), pp. 29–52.
[87]A. Domenicano, in *Stereochemical Applications of Gas-Phase Electron Diffraction, Part B*, edited by I. Hargittai and M. Hargittai (VCH, New York, NY, 1988), pp. 281–324.
[88]A. Domenicano, in *Accurate Molecular Structures: Their Determination and Importance*, edited by A. Domenicano and I. Hargittai (Oxford University Press, Oxford, 1992), pp. 437–468.
[89]J. Gauss and J. F. Stanton, J. Phys. Chem. A **104**, 2865 (2000).
[90]G. Portalone, G. Schultz, A. Domenicano, and I. Hargittai, Chem. Phys. Lett. **197**, 482 (1992).